

# Comparison of Sprinting With and Without Running-Specific Prostheses Using Optimal Control Techniques

Anna Lena Emonds<sup>†\*</sup> , Johannes Funken<sup>‡</sup>,  
Wolfgang Potthast<sup>‡</sup> and Katja Mombaur<sup>†</sup>

<sup>†</sup>*Optimization, Robotics and Biomechanics, Institute of Computer Engineering, Heidelberg University, Heidelberg, Germany.*

*E-mail: [katja.mombaur@ziti.uni-heidelberg.de](mailto:katja.mombaur@ziti.uni-heidelberg.de)*

<sup>‡</sup>*Institute of Biomechanics and Orthopaedics, German Sport University Cologne, Cologne, Germany.*

*E-mails: [j.funken@dshs-koeln.de](mailto:j.funken@dshs-koeln.de), [Potthast@dshs-koeln.de](mailto:Potthast@dshs-koeln.de)*

(Accepted May 25, 2019. First published online: July 2, 2019)

## SUMMARY

The purpose of our study was to get deeper insights into sprinting with and without running-specific prostheses and to perform a comparison of the two by combining analysis of known motion capture data with mathematical modeling and optimal control problem (OCP) findings. We established rigid multi-body system models with 14 bodies and 16 degrees of freedom in the sagittal plane for one unilateral transtibial amputee and three non-amputee sprinters. The internal joints are powered by torque actuators except for the passive prosthetic ankle joint which is equipped with a linear spring–damper system. For each model, the dynamics of one sprinting trial was reconstructed by solving a multiphase least squares OCP with discontinuities and constraints. We compared the motions of the amputee athlete and the non-amputee reference group by computing characteristic criteria such as the contribution of joint torques, the absolute mechanical work, step frequency and length, among others. By comparing the amputee athlete with the non-amputee athletes, we found reduced activity in the joints of the prosthetic limb, but increased torques and absolute mechanical work in the arms. We also compared the recorded motions to synthesized motions using different optimality criteria and found that the recorded motions are still far from the optimal solutions for both amputee and non-amputee sprinting.

**KEYWORDS:** Dynamics reconstruction; Amputee sprinting; Modeling; Optimization; Running-specific prostheses.

## 1. Introduction

Some sprinters with leg amputations have come remarkably close to the race times of their elite non-amputee colleagues, thereby drawing the attention to their running-specific prostheses and their impact on the sprinting performance. Each time that an athlete with leg amputation aimed to compete in the Olympic Games or another major athletic competition, this initiated a controversial discussion on whether sprinting with running-specific prostheses is advantageous or disadvantageous compared to sprinting with two biological limbs. Brüggemann and colleagues<sup>1</sup> analyzed one double below-knee amputee athlete and compared his sprinting biomechanics to that of a non-amputee reference group. They found that the amputee athlete relies on a completely different motion pattern caused by differences in the ankle joint moments and joint energy changes. These findings were confirmed

\* Corresponding author. E-mail: [annalena.emonds@ziti.uni-heidelberg.de](mailto:annalena.emonds@ziti.uni-heidelberg.de)

by Weyand et al.<sup>2</sup> But they found as well that the mechanical differences do not alter the sprinting physiology which is similar in double transtibial amputee and non-amputee sprinting. They posed the crucial question whether the amputee athlete's way of locomotion can still be classified as 'sprinting'. A similar statement was raised by Burkett et al.<sup>3</sup> saying that in a competition the athletes must clearly run and not bounce or hop. They further discussed ethical questions arising from the use of possibly advantageous running-specific prostheses. Several authors point to the difficulty of making general statements as only few amputee athletes compete at world level and they cannot be compared to themselves without an amputation.<sup>4-6</sup> This problem might be addressed, *inter alia*, by computer simulation of human sprinting: Mombaur<sup>7</sup> contributed to the discussion with the comparison of a double transtibial amputee athlete and a reference non-amputee athlete for whom only the prosthetic device model was replaced by thigh and foot models. By formulating an optimal control problem (OCP) with a torque minimizing objective function, it was shown that the torques and the absolute work were remarkably lower in the case of the double transtibial amputee athlete for the cyclic phase of running. But as a sprint competition consists of different race situations, all of them must be taken into account and judged in a balanced way. Studies on the sprint start<sup>8-10</sup> and curved sprinting<sup>11</sup> indicated that (unilateral) amputee athletes might have a disadvantage in these situations compared to non-amputee athletes.

Another unsettled issue is the question which criterion or which combination of criteria should be used for a comparison and a judgment of advantage or disadvantage. Although the basic biomechanics of sprinting is already rather well understood, it is difficult to tell what is optimized in sprinting, that is, which combination of optimality criteria is minimized or maximized by an elite sprinter. It seems obvious that a sprinter tries to run as fast as possible, thus maximizing the product of step length and step frequency.<sup>12,13</sup> Hobara and colleagues<sup>12</sup> found shorter step lengths in amputee sprinting compared to non-amputee athletes that lead to differences in sprint performance. In a different study, Hobara et al. reported differences in the stiffness regulation between the biological and the prosthetic leg of unilateral amputee sprinters.<sup>14</sup> Weyand and Bundle<sup>6</sup> worked out that the use of the light running-specific prostheses made from carbon-fiber allows double transtibial amputee athletes to achieve a higher step frequency. However, one can think of a number of other criteria that might be optimized in human sprinting – related to energy expenditure, stabilization and application characteristics – and are even harder to access. As an example, Kugler and Janshen<sup>15</sup> discussed the importance of body position and angular momentum in the acceleration phase of a sprint start. Willwacher et al.<sup>16</sup> found high free moments in high-speed running due to an insufficient cancellation of the angular impulses between upper and lower body. Weyand and colleagues<sup>17</sup> found that faster sprinters apply greater ground forces in shorter contact times compared to slower runners. Hence, a number of criteria exist and affect the sprint performance. In this study, we present a detailed comparison of characteristic properties that might influence sprint performance by evaluating reconstructed dynamic solutions of a least squares OCP. First results concerning the joint torques for one non-amputee and one amputee athlete have been presented before.<sup>18</sup>

Dynamic human motions are commonly analyzed based on kinematic motion capture recordings,<sup>1,17,19</sup> physiologic measurements,<sup>6</sup> video analysis<sup>12,13</sup> or combinations of those. If additional force plate data are available, a standard approach is an inverse dynamics analysis where joint moments are computed from a combination of external ground reaction forces, contact positions and pre-processed motion capture data. However, a common problem is the occurrence of high residual forces due to skin motion and wobbling masses. It becomes even more pronounced the more dynamic a movement is. Several approaches have been proposed to reduce the problem, for example, by modifying the marker post-processing<sup>20</sup> or by applying a residual reduction algorithm.<sup>21</sup> The need of a precise measurement of the ground reaction forces for the inverse dynamics approach is a further issue due to the fact that the number of force plates is often limited and often restricts the data capturing to indoor and/or laboratory conditions. Thus, having a valid method to calculate joint kinetics without measuring the ground reaction force would create great opportunities for researchers to analyze athletes more comprehensive under various conditions, for example, competitions or outdoor tracks. The least squares OCP formulation of this paper achieves a dynamics reconstruction with zero residual forces from purely kinematic data. The method has been successfully applied by Felis and colleagues<sup>22</sup> who reconstructed the dynamic walking gait of 15 motion capture recordings. Similar optimization-based approaches have been used by Lin and Pandy<sup>23</sup> to study muscle excitations of five subjects in walking and running or by Miller et al.<sup>24</sup> for the study of muscle mechanical properties in running.

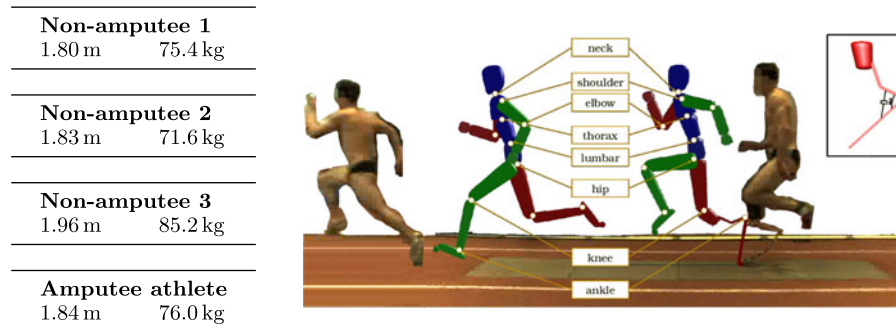


Fig. 1. Rigid multi-body system models of a non-amputee and an amputee athlete.

The remainder of this paper is structured as follows: In Section 2, we start with the description of the subject-specific rigid multi-body system models which we established for one unilateral transtibial amputee and three non-amputee athletes. We then present the mathematical formulation of sprinting motions. We continue with the description of the reference data generation that is based on motion capture recordings in Section 3. In Section 4, we finish the elaboration of our methods with the least squares OCP formulation that we used for the dynamics reconstruction of four individual sprinting motions. Finally, we present and discuss the numerical results of our computations with respect to differences in non-amputee and amputee sprinting (Section 5): In Section 5.1, we analyze the quality of the least squares fitting approach. A comparison of the phase durations, generalized coordinates and joint torque time histories between the amputee and the non-amputee athletes is presented in Section 5.2. Finally, characteristic parameters were computed for both the reconstructed solution and solutions optimizing a single optimality criterion. Sections 5.3 and 5.4 discuss differences in these measures. We conclude the discussion with a short summary and future work plans in Section 6.

## 2. Modeling Sprinting Motions With and Without Prostheses

For the investigation of sprinting motions with and without running-specific prostheses, we created subject-specific models of one unilateral transtibial amputee and three non-amputee athletes. For each, the rigid multi-body system model consists of 14 segments (head, upper and lower arms, three torso segments, thighs, shanks and feet/prosthetic device) with 16 degrees of freedom (DOFs) in the sagittal plane: Three global DOFs describe the position and orientation of the pelvis, which is used as the floating base of the model. The remaining 13 DOFs are associated with the rotations of the internal joints (see Fig. 1). We assume that the action of all related muscles is summarized by joint torque actuators in the internal joints. For the amputee athlete, the below-knee segments of the right leg are replaced by a model of the prosthetic device. It is coupled to the remaining part of the shank by a fixed joint. The real prosthesis has no ankle joint since it is made of compliant material which shows an overall deformation. In our model of the running-specific prosthesis, we approximate this behavior by replacing it by two rigid segments with a rotational joint in between such that the model has an ‘ankle joint’ on which a linear spring–damper system is acting. The point of the ankle joint is defined as the point of the prosthesis greatest curvature which, at the same time, is the most posterior point of the prosthesis.<sup>25</sup> The torque generation of the non-actuated prosthesis can be computed by

$$\tau_F(q, \dot{q}) = -d\dot{q} - k(q - \vartheta_0), \quad (1)$$

with  $q$ ,  $\dot{q}$  denoting the angle and the angular velocity in the prosthetic joint. The spring constant  $k$  and the damping constant  $d$  are free parameters of the optimization problem.  $\vartheta_0$  denotes the rest position of the spring. The subject-specific models are based on the de Leva data<sup>26</sup> which we extrapolated to the measured heights and masses of the individual athletes (cf. Fig. 1). The model of the prosthetic device was created according to measured data taken during the experiments described in Section 3.

We model the sprinting motions as a sequence of alternating flight and single-leg contact phases (see Fig. 2), each of which is described by its own set of ordinary differential equations (ODEs) or differential-algebraic equations (DAEs), as explained further in the following. Between the phases, discontinuities in the state variables can occur: Our assumption of a completely inelastic touchdown

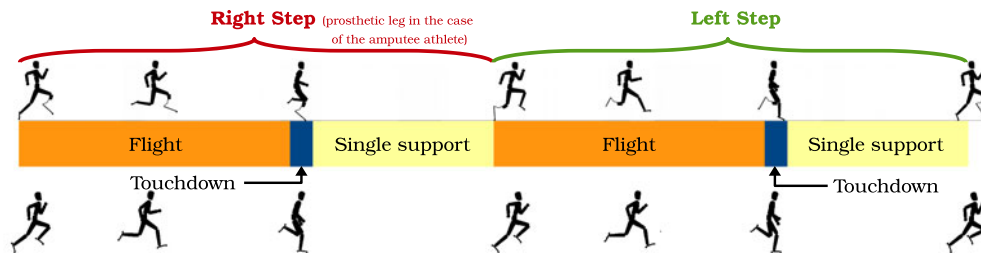


Fig. 2. Schematic representation of the subdivision of sprinting motions into phases.

results in discontinuities at velocity level. Due to the asymmetry between the biological and the prosthetic leg of the amputee athlete, we consider two full steps to investigate differences between them. A main characteristics of sprinting is that at higher velocities no flat foot ground contact occurs any more. This is taken into account by a point-like, rigid and non-sliding contact with the ball of the foot.

2.1. Equation of motion during the flight phase

During each of the two flight phases, the motion is described by a set of ODEs:

$$M(q) \ddot{q} + N(q, \dot{q}) = \tau, \tag{2}$$

where  $M(q)$  is the symmetric positive definite mass matrix containing the inertial properties of the system and  $N(q, \dot{q})$  is the vector of nonlinear effects such as the internal Coriolis, gyroscopic and centrifugal forces. All external forces including gravity, air friction as well as the torques generated by the muscles and the spring–damper system are stored in the vector of generalized forces  $\tau$ .

2.2. Equations of motion during the single-leg contact phase

Within the single-leg contact phase, the number of DOFs is reduced by two due to the non-sliding contact of the forefoot with the ground. To keep the same number of coordinates, we introduce an additional holonomic scleronomic constraint  $g(q) = 0$  with  $g : \mathbb{R}^{n_{dof}} \rightarrow \mathbb{R}^m$ , where  $m$  is the number of constraints. The equation of motion for a rigid multi-body model is then described by

$$M(q) \ddot{q} + N(q, \dot{q}) = \tau + G(q)^T \lambda, \tag{3a}$$

$$g(q) = 0, \tag{3b}$$

which is an index-3 differential-algebraic system.  $G = (\partial g / \partial q)$  is called contact Jacobian and  $\lambda \in \mathbb{R}^m$  denotes the contact forces. After differentiating the constraint equation (3) twice, we can rewrite the system as a linear system of the unknowns  $\ddot{q}, \lambda$ :

$$\begin{bmatrix} M & G^T \\ G & 0 \end{bmatrix} \begin{bmatrix} \ddot{q} \\ -\lambda \end{bmatrix} = \begin{bmatrix} -N + \tau \\ \gamma \end{bmatrix}. \tag{4}$$

The contact Hessian  $\gamma$  is calculated by differentiating the position constraints. If the constraints in  $g(q)$  are not redundant, the system is always solvable. At the beginning of the contact phase, the invariants of the constraints must be fulfilled to guarantee equivalence of (3) and (4):

$$g_{pos} = g(q(t)) = 0, \tag{5a}$$

$$g_{vel} = G(q(t)) \cdot \dot{q}(t) = 0. \tag{5b}$$

2.3. Discontinuities at touchdown

We model the touchdown of the foot as instantaneous and completely inelastic such that the body remains in contact with the ground and does not bounce off, ignoring the fast timescale effects of the real contact. Our previous research has shown that this is a very good approximation of the real behavior in the context of whole-body model running motion prediction.<sup>27</sup> Hence, the velocity of the contact point is instantly set to zero resulting in velocity discontinuities at touchdown. The change in the generalized velocities from  $v^-$ , the velocity before the collision, to  $v^+$ , the velocity after the collision, can be computed as

$$\begin{bmatrix} M & G^T \\ G & 0 \end{bmatrix} \begin{bmatrix} v_+ \\ \Lambda \end{bmatrix} = \begin{bmatrix} Mv_- \\ 0 \end{bmatrix}, \quad (6)$$

where we use the same matrices  $M$ ,  $G$  as above and  $\Lambda$  is the contact impulse.

Models of such complexity cannot be derived by hand. We use the Rigid Body Dynamics Library (RBDL)<sup>28</sup> to generate the equations of motions for our models.

#### 2.4. Initial, final and phase-switching conditions

For our sprinting model, we arrange the phases as shown in Fig. 2. To define proper ground contact as well as the events which prescribe touchdown and lift-off of the feet, we impose equality and inequality constraints that have to be satisfied by the model.

Each flight phase starts with the lift-off of the hallux contact point, at initial time  $h_0 = 0$ , at time  $h_3$  and at final time  $h_f$ , respectively. It occurs when the vertical ground reaction force becomes zero, that is,

$$F_z^{LH/RH}(x(h_i), u(h_i)) = 0, \quad (7)$$

where ‘LH’ and ‘RH’ denote the left and right hallux contact points, respectively. Touchdown occurs when the  $z$ -position of the hallux point equals zero and it is modeled by a transition phase. A second constraint guarantees that the foot does not move parallel to the ground or bounce up again, but is rigidly attached to the ground:

$$\begin{aligned} P_z^{LH/RH}(x(h_{i+1})) &= 0, \\ -V_z^{LH/RH}(x(h_{i+1})) &\geq 0. \end{aligned} \quad (8)$$

To make sure that the hallux point of the foot remains in contact with the ground during a contact phase, we require the vertical ground reaction force to be always positive:

$$F_z^{LH/RH}(x(h_i), u(h_i)) \geq 0. \quad (9)$$

### 3. Reference Data Generation from Motion Capture Experiments

For the dynamics reconstruction of sprinting motions as described in Section 4, we need reference sprinting data which is generated by extracting joint angle (and other relevant positional information) from the motion capture recordings.

The motion capture data were recorded as part of experiments at the German Sport University Cologne. The athletes were asked to perform sprint runs on an indoor athletics track. The motion capture system consists of a 3D camera system (VICON TM, Oxford, UK) comprising 16 infrared cameras operating at 250 Hz and four force plates (90 cm × 60 cm, Kistler, Winterthur, Switzerland) operating at 1250 (non-amputee athletes) or 1000 Hz (amputee athlete). The differences in the force sampling rates stem from the fact that the recordings for non-amputee and amputee athletes have been recorded within the scope of different projects. As we use the force data only for graphical comparison, the exact force sampling rate is not substantial. The force plates were built into the floor of the athletics track. For the motion recording, retro-reflective markers were placed on anatomic landmarks as well as the prosthetic device using adhesive tape. The markers that define the rotational joint of the running-specific prosthesis have been placed at the most posterior point of the prosthesis which at the same time is the point of the prosthesis’ greatest curvature.<sup>25</sup> Furthermore, the anthropometric data of the subjects and the mechanical properties of the running-specific prosthesis were documented.

To fit the marker positions of the recorded motions to the subject-specific models, we applied the tool Puppeteer<sup>22</sup> which computes the generalized coordinates of the model by an inverse kinematics fitting procedure. The resulting motion was used as a reference motion for the least squares dynamics fit described in the next section. All measured data were filtered using a fourth-order Butterworth filter with a cutoff frequency of 50 Hz. The phase durations corresponding to the phase segmentation of Fig. 2 were extracted by visually inspecting the kinematically fitted motions. If available, the force plate data were taken into account to approve the phase durations.

The dynamic data from the force plates were not used in the computations themselves, but will be only consulted as a reference in Section 5 to validate the quality of our results.

#### 4. Dynamics Reconstruction by an OCP Formulation

To perform a reconstruction of the full dynamics of the motion, using only reference kinematics for each subject without any force plate information, we formulate an OCP. This allows us to identify all joint torques with zero residual error as well as the ground reaction forces from the fact that ground contact is assured in the underlying dynamics by an appropriate constraint. The multiphase least squares OCP is formulated as follows:

$$\min_{x(\cdot), u(\cdot), p} \sum_{k=0}^m \frac{1}{2} \left( \|W (q_k^{MC} - q(h_k))\|_2^2 + \gamma_u \|u(h_k)\|_2^2 \right) \tag{10a}$$

subject to

$$\dot{x}(t) = f_i(t, x(t), u(t), p), \quad t \in [h_{i-1}, h_i], \tag{10b}$$

$$x(h_i^+) = c_i(x(h_i^-), p), \quad i = 1, \dots, m, \tag{10c}$$

$$g(t, x(t), u(t), p) \geq 0, \quad t \in [h_{i-1}, h_i], \tag{10d}$$

$$r^{eq}(x(0), \dots, x(h_f), p) = 0, \tag{10e}$$

$$r^{ineq}(x(0), \dots, x(h_f), p) \geq 0, \tag{10f}$$

where the differential state vector  $x(t)$  is composed by the generalized positions  $q(t) \in \mathbb{R}^{n_{dof}}$ , the generalized velocities  $\dot{q}(t) \in \mathbb{R}^{n_{dof}}$  and the joint torques  $\tau(t) \in \mathbb{R}^{n_{actuated}}$  of the model. The derivatives of the joint torques are used as control variables  $u(t) = \dot{\tau}(t)$ . The OCP is evaluated at time points  $h_i, i = 0, \dots, m$ . The number of time points is chosen per phase (52 time points in total: 15 points for each flight phase, 10 points for each contact phase, 1 point for each transition phase). The upper and lower bounds of the differential states  $x$ , the control variables  $u$  and the parameters  $p$  are specified in the path constraints (10d) and are chosen generously such that the reference movement can be smoothly tracked. Free parameters only occur in the case of the amputee model as the spring and damping constants of the prosthetic device are determined during the optimization routine. Since both of them have to be positive, the lower bounds are set to zero.

The objective function (10a) consists of two terms: The first one is the actual least squares term that minimizes the differences between the generalized coordinates of the model  $q(h_k)$  and those of the reference movement  $q_k^{MC}$ . It is weighted by the diagonal matrix  $W \in \mathbb{R}^{n_{dof}}$  with the weights chosen such that a close tracking of the generalized joint coordinates is achieved. As the motion capture data are recorded at a fixed sampling rate which might not coincide with the nodes of the OCP solver, it is interpolated by splines and evaluated at the nodes for the least squares method. The second term of the objective function is used to regularize the problem: By minimizing the squared control variables, it suppresses oscillations. The scaling factor  $\gamma_u$  guarantees that the least squares residuals contribute primarily to the objective function.

Equations (10b) and (10c) are placeholders for the full multiphase dynamics description including contact constraints as described in Section 2 (Eqs. (2)–(9)). The phase durations are fixed; each is prescribed by the original motion capture data. We decided on them by registering touchdown and lift-off events visually in the animated sequence (see Section 3) and, if available, verified the durations by adding the information of the vertical ground reaction force from force plate measurements.

The nonlinear point constraints (10e) and (10f) are used to formulate proper ground reaction forces and kinematic constraints such as touchdown and lift-off of the feet. They are evaluated as described in Section 2.4.

For the solution of the OCP, we use the software package MUSCOD-II developed at the Interdisciplinary Center for Scientific Computing Heidelberg.<sup>29,30</sup> It employs a direct method for control discretization and multiple shooting for state parametrization. The resulting large nonlinear programming problem is then solved by a specially tailored sequential quadratic programming method which applies condensing for the solution of each quadratic programming subproblem.

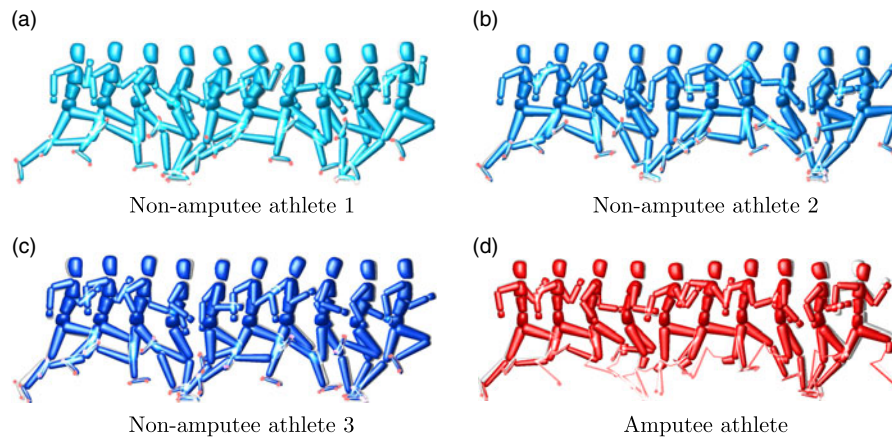


Fig. 3. Animated sequences of the reconstructed sprinting motions. The colored models illustrate the reconstructed motions, and the gray models in the background show the respective reference motions.

## 5. Numerical Results and Discussion

### 5.1. Analysis of the reconstruction quality and comparison to literature values

We reconstructed the sprinting dynamics of recorded motion capture trials for one amputee and three non-amputee athletes. If we refer to the ‘prosthetic ankle joint’ or the ‘ankle’ of the prosthetic leg in the following analysis, we mean the point of the prosthesis’ greatest curvature as described above. In Fig. 3, we show animated sequences of the reconstructed motions with colored models. The reference motions are animated in the background using a gray model.

The mean absolute error between the generalized coordinates of the kinematic reference data and the optimized solution has been calculated individually for each DOF. The optimal control based least squares fit yields a close tracking with mean absolute errors of less than 1.5 cm for the translational DOFs and less than  $1.2^\circ$  (0.02 rad) for the rotational ones. As the fit used for the reference motion generation does not include constraints, the reference data can still be unphysical; for example, the foot can penetrate the ground. In the reconstructed solution, such behavior is ruled out by the constraints of the OCP formulation. Obviously, this results in differences in the model poses between the reference and the reconstructed data at such points. They are the main contribution to the mean absolute errors.

The spring and damping constants of the prosthetic device have been free parameters of the optimization problem. We reconstructed a spring constant of 2737.5 N m/rad and a damping constant of 0.65 N m s/rad.

In Fig. 4, we compare the reconstructed ground forces to the filtered force plate measurements. The upper row depicts the horizontal ground forces and the lower row the vertical ground forces. The overall shape of the reconstructed ground forces matches the measurements well: For the horizontal force, all models reproduce a braking force in the first half of each contact phase and a following propulsive force. The timing of the transition between braking and propulsive force in the reconstructed data corresponds to the timing in the measured data. For the vertical component, all models produce parabolic shapes which are similar to both the measured ones and the vertical ground force shapes given in literature.<sup>31,32</sup> However, some features are not yet tracked perfectly by our models:

- The peak in the horizontal forces at the beginning of a contact phase is not reflected in the reconstructed solution.
- The model does not track the sharp increase in the vertical ground force of the non-amputee athlete 2.
- The model overestimates the propulsive component of the horizontal force during the first ground contact: The maximum value of the reconstructed solution is 38.5 % (NA1), 14.5 % (NA2), 23.4 % (NA3) and 17.1 % (amputee athlete) larger than the maximum value of the filtered measurement data. During the second ground contact, the model underestimates the propulsive component of the horizontal ground force for the non-amputee athlete 2 (74.0 % of the measured maximal value) and for the amputee athlete.

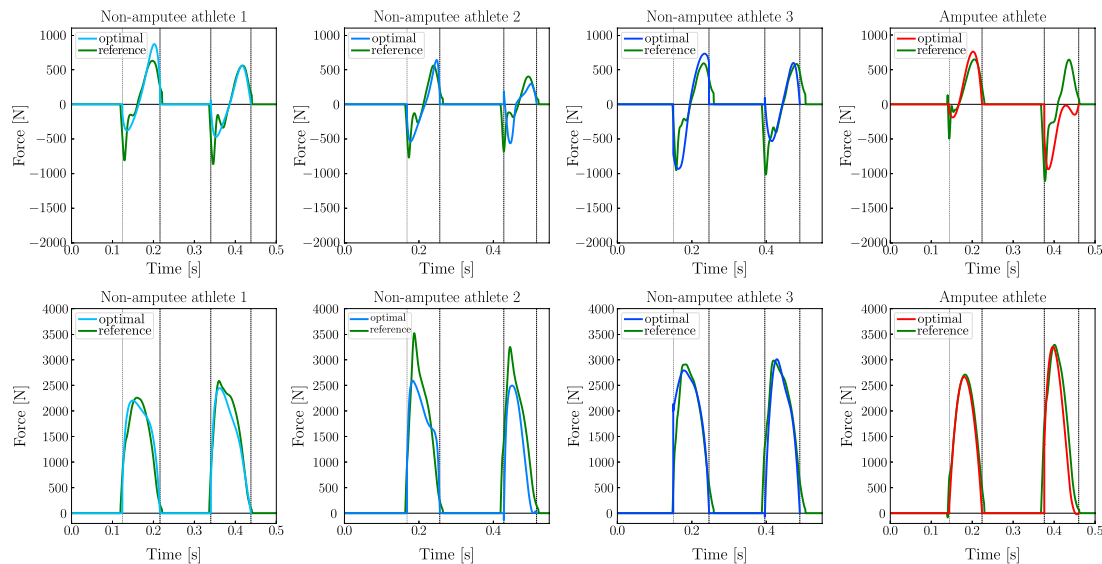


Fig. 4. Comparison of the computed and filtered measured horizontal (upper row) and vertical (lower row) ground reaction forces for the non-amputee and amputee athletes

All three effects might be a result of artifacts in the measurements. They further might result from our rather simple foot model with one fixed contact point per foot. In actual sprinting motions, the contact point travels along the hallux during contact. The first and the second effects might as well be due to the regularization term in the objective function (10a): The weight factor  $\gamma_u$  was chosen carefully in order to prevent that the minimization of the torque derivatives affects the solution. Nevertheless, it is possible that the energy loss due to a peak in the ground forces is impeded by the regularization term.

An advantage of our method is that we can compute external joint torques with zero residual forces from purely kinematic data because of our problem formulation. As we assume the action of all muscles at a joint to be summarized by joint torque actuators, we cannot distinguish between the individual contributions of the antagonist and the agonist muscle. Hence, all computed torques are net torques. As we are not interested in the individual contributions to the net torque in this analysis, a further subdivision was not necessary. The right half of Fig. 5 depicts the joint torque histories of both the non-amputee reference group and the amputee athlete. To our knowledge, no measured joint torques have yet been published for unilateral transtibial amputee sprinting. Nevertheless, to demonstrate that our approach computes realistic joint torques, we compare the results of the non-amputee athletes to joint torques for non-amputee sprinters from the literature.<sup>33–35</sup> Bezodis and colleagues<sup>33</sup> as well as Stafildis and Arampatzis<sup>34</sup> computed sagittal plane moments of the lower extremity joints during the stance phase of sprinting at velocities ranging from 9.06 to 10.37 m/s based on a standard inverse dynamics approach. We thus compare their data to the non-amputee histories of the contact leg segments during the respective contact phase. In the ankle, we found peak external flexion torques of around 5 N m/kg which match the results from the given literature. In the knee joints, we computed absolute external flexion torques of 1 N m/kg for the maximal extension torque and 3 N m/kg for the maximal flexion torque. They span a similar range as in refs. [33, 34] ( $\pm 2.5$  N m/kg for both extension and flexion moments). For the hip joint, Bezodis and colleagues<sup>33</sup> report a peak at the beginning of the contact phase which is not reflected in our data set. However, the joint torques are of comparable magnitude except for that peak. Furthermore, the overall trend from external flexion to external extension torques is the same. We would have expected that the left hip joint torque is more clearly in the negative half at the end of the left contact phase. We assume that this is due to the regularization term: Although it is chosen to be subdominant, it seems that the optimization exploits gravity for the end pose and drops the model down. This might be beneficial for minimizing the cost function and could be a reason for a discrepancy in the left hip torque and in the contact forces, as stated above. Schache and coworkers<sup>35</sup> presented similar torques during the ground contact phase of sprinting at  $(8.95 \pm 0.70)$  m/s. They additionally showed joint torques

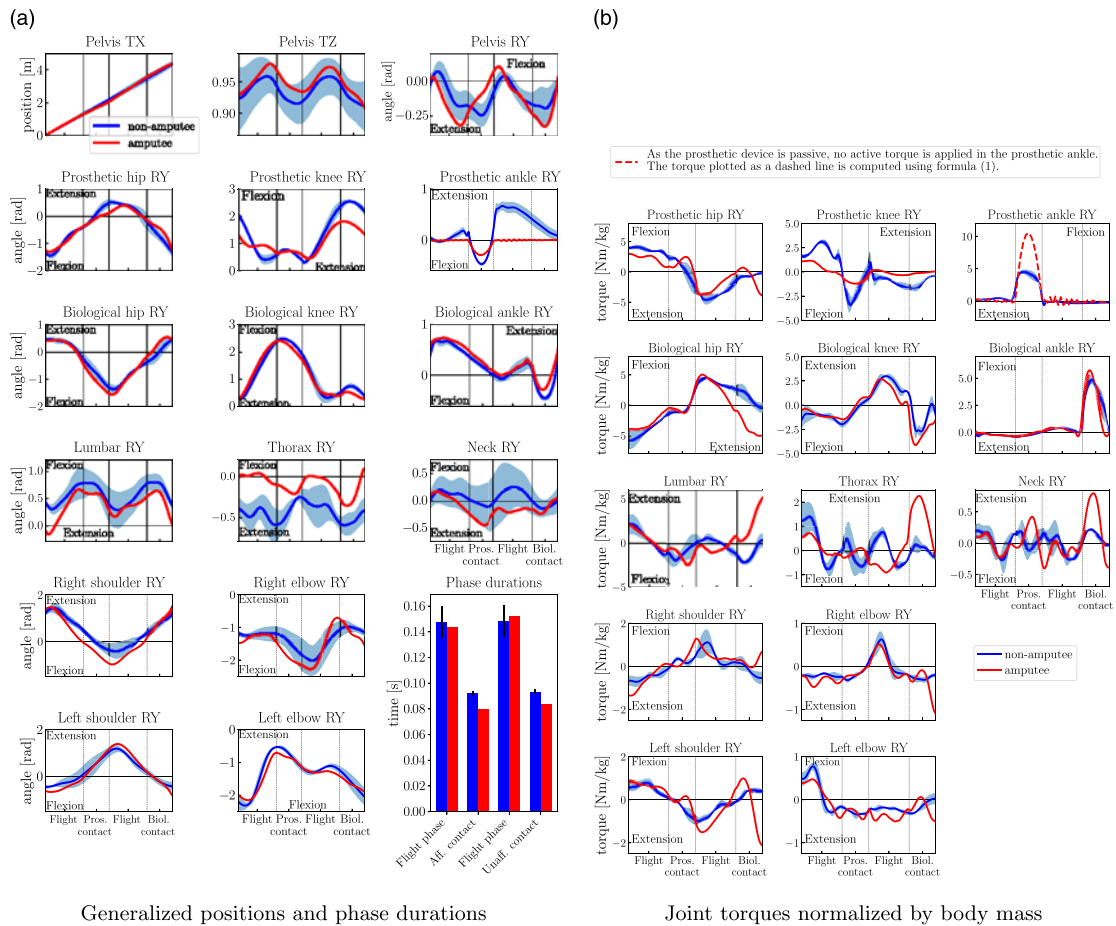


Fig. 5. Comparison of the generalized positions and phase durations as well as joint torques normalized by body mass between the amputee and the non-amputee athletes. The individual phase durations are scaled to make the different solutions comparable. The distinction between prosthetic and biological leg is made for the amputee athlete; for the non-amputee athletes, the corresponding biological leg is taken. For the amputee athlete, ankle refers to the point of the prosthesis' greatest curvature.

during the swing phase which are comparable to our reconstructed torques. The ankle and knee joint torques of the prosthetic leg of the unilateral amputee athlete in our computations are similar to those of a double transtibial amputee athlete.<sup>1</sup> However, Brüggemann and coauthors reported a maximum flexion torque of about 6.5 N m/kg in the prosthetic ankle joint which is smaller than the computed prosthetic ankle joint torque of the unilateral amputee athlete (around 11 N m/kg). The hip joint torques of the prosthetic side of the unilateral amputee athlete span a similar range of magnitude as those of a double transtibial amputee athlete,<sup>1</sup> but their curves differ clearly. This might be explained by the differences between unilateral and double amputee sprinting that are expectable due to the disparity in lower limb weight and leg stiffness.<sup>36</sup>

In summary, the fitting errors are rather small, the computed ground forces match the measured ones and the torques of the non-amputee athletes are comparable to those reported in the literature. These findings demonstrate the strength of our optimization-based approach for the dynamics reconstruction of purely kinematic data. As it does not require force plate measurements, it is helpful for the analysis of movements where no force plate data can be recorded (e.g. for outside measurements with a mobile motion capture system) or the measured force data contains errors. Furthermore, we can fit to all markers in a balanced way, thus eliminating any unfavorable error propagation along the kinematic chain.

Hence, the computed solutions allow for a further analysis and comparison of sprinting with and without prostheses. To state if a curve or a value is of comparable size or not, we define the following criteria: The value of the amputee athlete is significantly smaller/larger compared to the value of the non-amputee reference group if

1. the value is 15 % smaller/larger than the average value of the non-amputee athletes and the value is outside the single standard deviation or
2. the value is outside the twofold standard deviation of the non-amputee athletes.

Obviously, we cannot make any general statements on amputee and non-amputee sprinting as we only considered one trial of one amputee athlete and one trial for each of the reference group of three non-amputee athletes. Since the joint torques of the non-amputee athletes are in accordance with the literature, it is reasonable to expect that the joint torques of the amputee athlete might be confirmed by an inverse dynamics analysis in the future. Nevertheless, we do not want to make a general judgment on advantage or disadvantage in amputee sprinting with the following analysis, but we aim to contribute to the ongoing discussion. We want to demonstrate that optimal control-based motion reconstruction is a useful tool to get insight into the biomechanics of human sprinting from a different perspective and to analyze the solutions with respect to characteristic criteria for a reasonable judgment.

### 5.2. Analysis of phase durations, joint angle and torque histories and related quantities in non-amputee and amputee sprinting motions

The phase durations, generalized coordinates and joint torques of the amputee athlete are compared to those of the non-amputee athletes in the diagrams of Fig. 5: They show the curve shapes for two full steps starting and ending with the lift-off from the biological leg. As the individual phase durations differ among the athletes, we normalized them to make the curves comparable. The mean value of the three solutions of the non-amputee athletes is shown instead of the individual curves (blue solid line). The shaded regions indicate the standard deviation.

The flight phases are of comparable duration for both the amputee and the non-amputee athletes. The contact phase durations are smaller in the case of the amputee sprinter. Hence, the amputee athlete has a shorter step duration in total, that is, a higher step frequency. As the horizontal distance traveled by the floating base per step (see diagram for Pelvis TX) is comparable for both, the amputee athlete has a higher running velocity (9.61 m/s) compared to the non-amputee athletes ( $9.11 \pm 0.30$  m/s). The vertical movement of the floating base segment (Pelvis TZ) is similar for both groups.

As expected, the crucial differences between non-amputee and amputee sprinting become apparent in the joints of the lower extremity (hip, knee, ankle): In the case of the athlete with unilateral below-knee amputation, we find less extension and flexion for the knee and ankle joints of the prosthetic side. In particular, the range of motion in the knee of the prosthetic leg is much smaller. Less knee flexion has been reported for a double amputee athlete before.<sup>1</sup> It should be noted that the range of motion in the ankle of the amputee and the non-amputee athletes cannot be directly compared to each other due to the differences in the geometry of the prosthesis and the biological foot. The range of motion of the prosthetic side's hip of the amputee athlete is the same as for the hips of the non-amputee athletes. Maximum extension, though, only occurs in the middle of the flight phase in the case of the unilateral amputee athlete. In contrast, the non-amputee athletes extend their hips at the end of the prior contact phase. The joint angle histories of the hip and knee of the biological leg do not differ too much from the joint angle histories of the non-amputee athletes. Nevertheless, they are often at the edge of the standard deviation region of the non-amputee athletes.

Further differences can be found in the time histories of the arms: The amputee athlete has a larger range of motion in the shoulder joints which might be necessary to reach the sprint velocity and to compensate the inter-limb weight and stiffness asymmetry. The smaller joint angles in the spinal and neck segments indicate a more upright position of the amputee athlete compared to the non-amputee reference group. However, as the lumbar and thorax joint curves of the non-amputee athletes have similar values with opposite signs, they cancel each other partly.

These observations are reflected in the joint torque histories as well: The amputee sprinter applies significantly smaller torques in the knee of the prosthetic leg compared to the non-amputee athletes. Although one should keep in mind that the knee is affected by the amputation as well, it seems that athletes with below-knee amputation use a strategy to reduce external sagittal plane knee moments in order to optimally exploit the spring-like properties of the prosthesis. The hip joint torques of the prosthetic side are smaller, too, except for the prosthetic contact phase where the amputee athlete

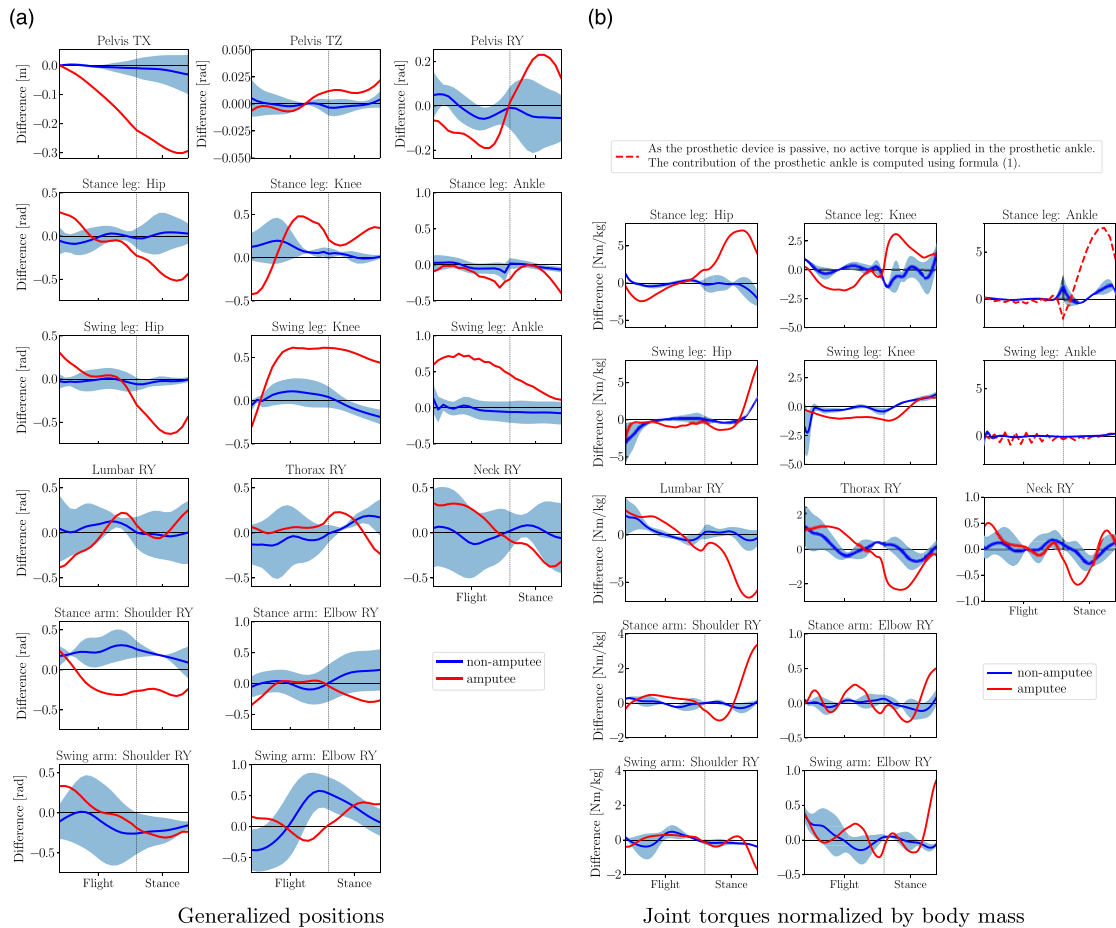


Fig. 6. Differences between the generalized positions and joint torques normalized by body mass of the two steps for amputee and non-amputee sprinting. For the joints where a left and a right segment exist, we subtracted the second step of the left segment from the first step of the right segment and vice versa. The label ‘Stance leg/arm’ denotes the side of the body that is in contact with the ground during the step.

has to apply a much larger torque to bring his hip forward. Despite the fact that the amputee athlete produces an external flexion torque during this contact phase, the hip extension torque in the prosthetic leg at the end of the phase is nearly identical for both groups. As the running-specific prosthesis is a passive device, no torque is produced actively by torque actuators in the prosthetic ankle (see Section 2). We computed the acting passive torque (dashed line) based on formula (1) with the spring and damping constant as calculated by the OCP. The torque produced by the passive prosthetic device doubles the ankle joint torques of the non-amputee reference group. This is easily understandable by considering the geometry of the running-specific prosthesis. Due to its length, the long lever arm produces large torques already from rather small joint angles and angular velocities. The torques produced in the biological leg of the amputee athlete are of similar magnitude as the leg joint torques of the non-amputee athletes. Within the contact phase of the biological leg, the joint torques of the amputee athlete are a bit larger than the corresponding torques of the non-amputee athletes. Similarly, larger torques occur in the arm joints of the amputee athlete compared to the non-amputee reference group, especially within and directly after the contact phase with the prosthetic leg. Hence, it might be that the action of the arms is used to compensate for differences occurring due to the amputation and the use of a running-specific prosthesis.

The diagrams of Fig. 6 show the differences in the time histories of the generalized coordinates and the joint torques between the two steps. The differences were computed by subtracting the second step (flight phase from prosthetic to biological leg and contact phase of the biological leg) from the first step (flight phase from biological to prosthetic leg and contact phase of the prosthetic leg). We took into account that the contact phases of the respective legs are shifted by one step and adjusted

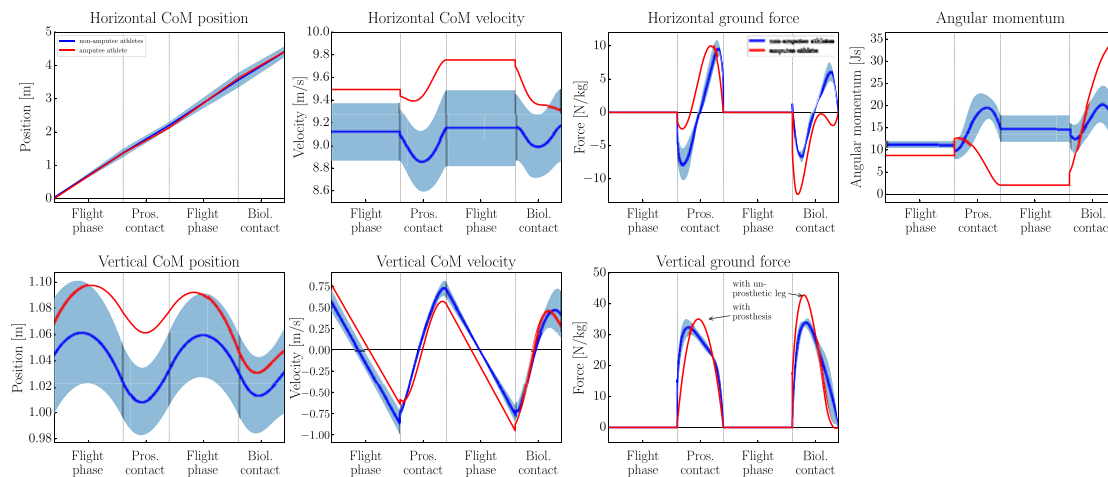


Fig. 7. Comparison of characteristic quantities between a unilateral amputee athlete and the mean of three non-amputee athletes computed from least squares OCP solutions: CoM position, CoM velocity, ground reaction force and angular momentum (from left to right). For the first three quantities, the upper row depicts the horizontal component and the lower row depicts the vertical component.

them for the subtraction such that the touchdown events coincide. If the curve of a specific joint is close to zero, the movement of the joint is rather symmetric during two subsequent steps. Thus the diagrams depict a measure of how symmetric the time histories are. As expected, the inter-limb asymmetry of the amputee athlete becomes apparent in these diagrams. In total, the curves of the non-amputee athletes are closer to zero than those of the amputee athlete indicating that he has a more asymmetric style of sprinting. At the end of the step, the deviation of the horizontal floating base displacement is about 30 cm. The floating base covers a shorter distance during the first step (flight phase from biological to prosthetic leg and contact phase of the prosthetic leg). It is interesting that the difference in step lengths between those steps (16 cm, see Table I) only amounts half of this value. Furthermore, major deviations can be found in the joint angles of the legs. The differences between the first and second steps of the amputee athlete have absolute values of around  $0.5 \text{ rad} \approx 28^\circ$ . The deviations in the leg joints of the non-amputee athletes are much smaller (approx.  $0.15 \text{ rad} \approx 8^\circ$ ). The differences in the joint torques of the prosthetic leg of the unilateral amputee athlete are large as well (between 2 and 7 N m/kg).

In Fig. 7, we juxtapose further relevant quantities, namely the horizontal and vertical center of mass (CoM) positions, CoM velocities and ground reaction forces and the angular momentum with respect to the CoM. Within the prosthetic leg contact phase, the vertical CoM position of the amputee athlete is higher compared to the non-amputee athletes. The braking and propulsive components of the horizontal ground forces are approximately symmetric for the non-amputee sprinters. It must be taken into account that the difference in the propulsive components probably is due to the fact that the model does not perfectly reconstruct them (cf. Section 5.1). Compared to these non-amputee reference curves, the amputee athlete applies less braking and more propulsive force during the prosthetic-side contact, whereas the opposite is true for the biological-side contact. The vertical ground reaction force of the amputee athlete during the contact with the biological leg is around 10 N/kg (30 %) larger than the force of the non-amputee reference group. Still, it must be taken into account that the diagrams of Fig. 7 are normalized per phase and that the amputee athlete applies the force in a shorter period of time. Hence the resulting change of vertical momentum is similar for both groups (compare Table I), which also fits to the fact that the flight phases are of similar duration. We conclude that the amputee athlete has to apply more ground force during the contact with the biological leg to run at a similar average velocity as the non-amputee reference athletes. The behavior of the angular momentum with respect to the CoM differs significantly within the contact phase with the prosthetic leg and the subsequent flight phase between the amputee athlete and the non-amputee athletes: The angular momentum of the non-amputee athletes increases and decreases during the contact, similar to the shape of the horizontal component of the ground reaction force. In the case of the non-amputee athletes, the angular momentum decreases during the contact phase to a quarter of the value of the previous flight phase (2.5 vs. 10 J/s).

### 5.3. Analysis of measures related to effort, energy expenditure and sprinting style

To compare the sprinting motions from a different perspective, we have computed criteria related to effort, energy expenditure, contact event timing and sprinting style which might be minimized or maximized by a sprinter. All torques and forces were normalized by the individual body mass  $M$  such that  $\tau_i^* = \frac{\tau_i}{M}$ ,  $f_{h/v}^* = \frac{f_{h/v}}{M}$ ,  $E_{\text{kin}/\text{pot}}^* = \frac{E_{\text{kin}/\text{pot}}}{M}$  and  $l_y^* = \frac{l_y}{M}$ . The computational results of the following criteria are given in Table 1:

- the average over both the absolute and the squared values of the joint torques per distance traveled:  $\frac{1}{TD} \int_0^T |\tau_i^*| dt$  and  $\frac{1}{TD} \int_0^T (\tau_i^*)^2 dt$ ,
- the average over both the absolute and the squared values of the joint torque derivatives per distance traveled:  $\frac{1}{TD} \int_0^T |\dot{\tau}_i^*| dt$  and  $\frac{1}{TD} \int_0^T (\dot{\tau}_i^*)^2 dt$ ,
- the absolute mechanical work of each joint per distance traveled:  $\frac{1}{D} \int_0^T |\tau_i^* \dot{\phi}_i| dt$ ,
- the average over the joint powers per distance traveled:  $\frac{1}{TD} \int_0^T (\tau_i^* \dot{\phi}_i) dt$ ,
- the relative contact time:  $t_{\text{contact}}/t_{\text{step}}$ ,
- the step frequency:  $f_{\text{step}}$  (where one step consists of one flight and one contact phase),
- the step length:  $d_{\text{step}}$ ,
- the average horizontal velocity of the floating base segment:  $\overline{v_{h,\text{pelvis}}}$ ,
- the horizontal change of momentum normalized by body mass:  $\int_0^T f_h^* dt$ ,
- the mean horizontal force normalized by body mass:  $\overline{f_h^*}$ ,
- the vertical change of momentum normalized by body mass:  $\int_0^T f_v^* dt$ ,
- the mean vertical force normalized by body mass:  $\overline{f_v^*}$ ,
- the vertical peak force normalized by body mass:  $(f_v^*)_{\text{max}}$ ,
- the average over both the absolute and the squared angular momentum with respect to the CoM:  $l_y$ :  $\frac{1}{T} \int_0^T |l_y^*| dt$  and  $\frac{1}{T} \int_0^T (l_y^*)^2 dt$ ,
- the average over both the absolute and the squared head orientation:  $\frac{1}{T} \int_0^T |\varphi_{\text{head}}| dt$  and  $\frac{1}{T} \int_0^T \varphi_{\text{head}}^2 dt$ ,
- the average over both the absolute and the squared head angular velocity:  $\frac{1}{T} \int_0^T |\dot{\varphi}_{\text{head}}| dt$  and  $\frac{1}{T} \int_0^T (\dot{\varphi}_{\text{head}})^2 dt$ ,
- the average over the kinetic energy per distance traveled:  $\frac{1}{TD} \int_0^T E_{\text{kin}}^* dt$  and
- the average over the potential energy per distance traveled:  $\frac{1}{TD} \int_0^T E_{\text{pot}}^* dt$ .

The total time is denoted by  $T$  and the distance traveled by the floating base segment is denoted by  $D$ . We computed the average values for both the absolute and the squared quantities because the squared values in combination with the absolute values give information whether the curve has peaks or is at a rather uniform level. All integrals are computed approximately using information at the multiple shooting points. If applicable, the results are given for each joint separately. In addition, we computed the sum over all joints except for the joint powers. As positive and negative values exist, which cancel out each other in the computations, a sum would be meaningless due to the fact that negative joint power in a joint does not imply an energy gain in reality.

We now go through the table systematically to emphasize significant differences: The first part gives the values related to joint torques. For both the absolute and the squared values, the sum over all joints is much smaller for the amputee athlete than the non-amputee references meaning that the model applies less torque per distance and body mass. However, for the individual joints, we observe all three possible cases: torques that are larger for the amputee athlete (left arm), torques that are smaller (prosthetic leg) and torques that are of similar size (biological leg, spinal joints, right arm). This confirms the findings of the diagrams in Fig. 5. In the next part of the table, the joint torque derivatives are considered. In contrast to the torques, the sum over all joints yields comparable orders of magnitude meaning that the rate of change of the torques is similar for both groups. Interestingly, this is not the case for the individual joints: The values related to the torque derivatives of the amputee athlete are much larger than or comparable to the values for the non-amputee athletes. Only the value corresponding to the knee joint of the prosthetic leg is very small (30%/8% of the non-amputee

Table I. Comparison of characteristic values between the amputee and the non-amputee athletes. The criteria for which the computed value of the amputee athlete is much smaller than the one of the non-amputee reference groups is indicated by the red background. The blue background indicates the opposite effect. In the table, we use the following abbreviations: A – amputee athlete, NA – average of non-amputee athletes, R – right side of the body (prosthetic leg side), L – left side of the body.

Joint	NA	A–R	A–L	NA	A–R	A–L
	Absolute torques [N/kg]			Squared torques [N <sup>2</sup> m/kg <sup>2</sup> ]		
normalized to total body mass [kg] and traveled distance [m]						
Hip	0.62 ± 0.04	0.44	0.62	2.19 ± 0.28	1.10	2.26
Knee	0.34 ± 0.03	0.10	0.33	0.68 ± 0.10	0.08	0.70
Ankle	0.21 ± 0.03		0.17	0.64 ± 0.15		0.58
Shoulder	0.10 ± 0.01	0.11	0.16	0.07 ± 0.02	0.08	0.16
Elbow	0.06 ± 0.01	0.07	0.07	0.020 ± 0.004	0.03	0.03
Lumbar	0.23 ± 0.05		0.26	0.39 ± 0.15		0.57
Thorax	0.12 ± 0.01		0.13	0.11 ± 0.05		0.15
Neck	0.04 ± 0.01		0.05	0.010 ± 0.003		0.02
Sum	3.04 ± 0.12	2.51		7.72 ± 0.69	5.77	

Joint	Absolute torque derivatives [N/(kg s)]			Squared torque derivatives [N <sup>2</sup> m/(kg s <sup>2</sup> )]		
	normalized to total body mass [kg] and traveled distance [m]					
Hip	7.30 ± 0.64	9.82	10.45	476 ± 85	930	903
Knee	9.21 ± 1.35	2.42	7.74	955 ± 420	52	760
Ankle	5.91 ± 0.71		7.41	939 ± 170		1141
Shoulder	2.35 ± 0.54	2.57	4.27	46 ± 19	48	171
Elbow	1.36 ± 0.16	1.94	1.74	20 ± 6	30	19
Lumbar	6.98 ± 1.50		7.64	332 ± 116		435
Thorax	4.88 ± 0.18		4.18	168 ± 21		178
Neck	1.81 ± 0.40		2.52	26 ± 11		53
Sum	65.9 ± 3.8		62.7	5397 ± 931		4721

Joint	Absolute mechanical work [J/(kg m)]			Joint powers [W/(kg m)]		
	normalized to total body mass [kg] and traveled distance [m]					
Hip	1.92 ± 0.09	1.55	2.16	3.15 ± 0.25	2.12	1.84
Knee	1.75 ± 0.22	0.25	1.43	−2.73 ± 0.31	−0.29	−2.26
Ankle	0.99 ± 0.09		0.73	−0.23 ± 0.10		−0.65
Shoulder	0.32 ± 0.06	0.44	0.61	−0.01 ± 0.13	0.52	0.46
Elbow	0.20 ± 0.04	0.24	0.17	0.12 ± 0.08	0.20	0.10
Lumbar	0.52 ± 0.01		0.97	−0.14 ± 0.37		−0.83
Thorax	0.19 ± 0.04		0.22	0.01 ± 0.20		0.21
Neck	0.06 ± 0.01		0.08	0.04 ± 0.04		0.03
Sum	11.1 ± 0.5	8.9				

Table I. Continued.

	NA	A	NA	A	NA	A
	Right step (pros. leg)		Left step (biol. leg)		Average for both steps	
Rel. cont. time	0.39 ± 0.03	0.36	0.39 ± 0.04	0.36	0.39 ± 0.03	0.36
Step frequency [Hz]	4.20 ± 0.31	4.46	4.15 ± 0.27	4.24	4.17 ± 0.21	4.35
Step length [m]	2.18 ± 0.06	2.10	2.18 ± 0.05	2.24	2.180 ± 0.003	2.18
Average vel. [m/s]	9.09 ± 0.23	9.16	9.14 ± 0.38	9.87	9.11 ± 0.30	9.52
Horizontal change of momentum [N s/kg]	0.06 ± 0.12	0.32	0.02 ± 0.03	-0.37	0.06 ± 0.05	-0.03
Hor. mean force [N/kg]	0.64 ± 1.33	3.96	0.20 ± 0.28	-4.45	0.42 ± 0.68	-0.49
Vertical change of momentum [N s/kg]	2.32 ± 0.17	1.89	2.01 ± 0.24	1.95	2.17 ± 0.15	1.92
Vert. mean force [N/kg]	25.3 ± 1.8	23.6	21.6 ± 2.0	23.2	23.4 ± 1.3	23.4
Vert. peak force [N/kg]	32.7 ± 2.8	35.1	34.2 ± 1.3	42.8	33.5 ± 1.6	39.0
	NA	A	NA	A		
	Absolute values		Squared values			
Angular momentum [J s]	0.19 ± 0.02	0.12	0.04 ± 0.01	0.03		
Head orientation [rad]	0.20 ± 0.02	0.12	0.06 ± 0.01	0.02		
Head velocity [rad/s]	3.67 ± 0.25	3.49	21.6 ± 3.1	17.3		
Kin. energy [J/(kg m)]	10.21 ± 0.93	10.99				
Pot. energy [J/(kg m)]	2.32 ± 0.07	2.38				

athletes for the absolute/squared value). The small value shows that the torque hardly changes over the steps and that the knee of the prosthetic side is affected by the amputation as well.

The significantly smaller values in the prosthetic leg of the amputee athlete compared to the non-amputee reference group are reflected in the absolute mechanical work in the respective joints as well: The amputee athlete produces about 80 % of the mechanical work achieved by the non-amputee athletes in the hip and less than 20 % in the knee of the prosthetic side. While this might be partly due to the use of a running-specific prosthesis, it is reasonable to presume that the capability of the residual limb is diminished by the below-knee amputation (especially in the knee joint). However, it appears that athletes with a below-knee amputation adopt a strategy that increases the load on the carbon fiber prosthesis by decreasing the load on the biological tissues of the residual limb. This results in a reduced absolute mechanical work in the respective joints as well. For the biological leg, less work is applied in the knee joint (79 % of the non-amputee mean value) whereas in the hip and ankle approximately the same amount of mechanical work is produced. The absolute mechanical work is clearly larger in the shoulder joints. It might be that more work is needed to compensate the inter-limb asymmetry.

The average over the joint powers in each joints indicates if the energy absorption (negative value) or generation (positive value) prevails in average. The values related to phase duration relative to the total step duration, step frequency, step length and average velocity have already been discussed in Section 5.2.

The next section of the table introduces quantities related to the ground reaction forces and the change of momentum due to them. Major differences between the amputee and the non-amputee athletes can be found in the horizontal components: During the prosthetic contact phase, the horizontal change of momentum is clearly deviating from zero. Thus, the propulsive force exceeds the braking force. The horizontal change of momentum is close to zero for both contact phases of the

Table II. Comparison of characteristic values of sprinting between the reconstructed solution and solutions optimizing a single criterion for the non-amputee athlete 1 and the amputee athlete

Criterion	Non-amputee athlete 1		Amputee athlete	
	reconstructed from Table I	optimized from ref. [37]	reconstructed	optimized from ref. [37]
Min. torques	$\min \int_0^T \tau_i^2 dt$			
- Sum abs. torques	3.03	1.64	2.51	1.12
- Sum sq. torques	7.22	2.73	5.77	1.16
Min. torque derivatives	$\min \int_0^T \dot{\tau}_i^2 dt$			
- Sum abs. torque derivatives	70.3	27.5	62.7	21.3
- Sum sq. torque derivatives	5177	1274	4721	580
Min. work	$\min \int_0^T  \tau_i \dot{\phi}_i  dt$			
- Sum abs. mech. work	10.55	3.44	8.90	3.53
Min. angular momentum	$\min \int_0^T l_y^2 dt$			
- Average abs. ang. mom.	0.16	$3.1 \times 10^{-4}$	0.12	$4.1 \times 10^{-4}$
- Average sq. ang. mom.	0.03	$9.1 \times 10^{-7}$	0.03	$9.9 \times 10^{-7}$
Min. rel. contact time	$\min t_{\text{contact}}/t_{\text{step}}$			
- Average rel. cont. time	0.43	0.28	0.36	0.32
Max. step frequency	$\min - \dot{f}_{\text{step}}$			
- Average step frequency	4.57	5.72	4.35	4.61
Max. step length	$\min - \dot{d}_{\text{step}}$			
- Average step length	2.11	3.00	2.18	2.50

non-amputee athletes, which means that the propulsive and braking forces balance each other. This behavior meets our expectations. Although it must be taken into account that the reconstruction of the horizontal forces did not correspond to the measured data perfectly (cf. discussion of Fig. 4), it is obvious that the horizontal change of momentum varies a lot between the two steps of the amputee athlete. A similar observation results from the comparison of the horizontal mean force. The difference between the mean force during the prosthetic-leg and the biological-leg contact phase cannot be explained solely by weak points of the reconstruction. The clearly higher vertical mean and peak forces of the amputee athlete that occur within the contact of the biological leg are applied during a shorter contact time. This explains why the vertical change of momentum is of comparable magnitude for both groups.

The values computed for angular momentum, head orientation and head velocity are all related to the overall posture and the change in it. The amputee athlete has much smaller values for all three criteria, thus indicating that he runs in a more upright position which we already concluded from the visual impression of Figs. 3 and 5.

5.4. Comparison of measures related to effort, energy expenditure and sprinting style to synthesized solutions optimizing a single criterion

To conclude the evaluation of the numerical results, we briefly want to compare the reconstructed solutions to OCP solutions which optimize single criteria related to sprinting effort and performance. In a study on optimality criteria in sprinting,<sup>37</sup> we synthesized sprinting motions with and without running-specific prostheses based on 10 criteria including the minimization of joint torques, torque derivatives, angular momentum and maximization of step length and frequency. In this study, the models of the non-amputee athlete 1 and the amputee athlete have been used. We computed the quantities from Table I that are related to the respective optimality criterion in order to compare the results to the reconstructed dynamics. The values are presented in Table II.

The first three criteria (minimization of joint torques, joint torque derivatives and absolute mechanical work per joint) are quantities related to the effort of sprinting motions. The angular momentum minimization enforces minimal rotations of the model over the CoM. It is apparent that the solutions optimizing single criteria yield values which are much smaller than those of the recorded motions – for both the non-amputee and the amputee athletes. Hence, neither the non-amputee nor the amputee athlete tries to solely minimize the effort during the steady-state phase of sprinting. This in turn means that the real amputee athlete does not exploit the theoretical potential of his running-specific prosthesis in terms of effort reduction to the same extent as the model of the optimization.

The last three criteria (minimization of relative contact times, maximization of step frequency and length) are measures of sprinting performance. Again, the reconstructed solution from the motion capture experiments is still far away from the optimal solutions. This indicates that both athletes could in theory perform better. However, a deeper investigation including more detailed models with muscular properties is necessary for more quantitative statements. Furthermore, the table suggests that the athletes in reality do not optimize a single criterion, but a combination of them. A first step toward the identification of combinations that come close to the recorded motions using inverse optimal control has been taken in ref. [38].

## 6. Conclusion

We presented a dynamics reconstruction including joint torques of non-amputee and amputee sprinting and compared characteristic criteria in terms of energy efficiency and sprinting mechanics. We demonstrated the usefulness of combining mathematical modeling and optimal control for a deep investigation of practical motion capture recordings: The rigid multi-body system models were able to reconstruct characteristic dynamic quantities of sprint motions including joint torques and ground reaction forces. Hence, this approach is of particular interest for motions where force plate data are not available or have errors. We showed that a comparison of several criteria related to effort, performance and sprinting style yields significant differences between unilateral transtibial amputee and non-amputee sprinting. In some joints, the amputee athlete produces clearly less torques and absolute mechanical work than the non-amputee athletes. However, other criteria (e.g. related to the arm motion) indicate that the amputee athlete has to produce larger torques in some of the remaining joints. Still, the goal in a sprinting competition is to run as fast as possible and measures related to effort should not be the only criterion taken into a consideration. A future goal of our research is to use inverse optimal control to identify which combination of criteria is optimized during the steady-state phase of sprinting.

In general, it must be taken into account that it is obviously not sufficient to consider nothing but the steady-state phase of sprinting to discuss possible advantages or disadvantages of sprinting with running-specific prostheses. The design of the prosthetic device might be optimized for sprinting at a specific velocity which in turn means that it might cause difficulties for other velocities or during an acceleration phase. We therefore aim to extend our investigation to other race situations (e.g. acceleration and deceleration phases) and to study the parameters of the prosthetic device in different situations.

Finally, the evaluation of the numerical results has shown that the amputee athletes applies larger torques and mechanical work in the arm joints than the non-amputee athletes. He further rotates less around the CoM compared to them. In sprinting, the arms provide important assistance for keeping balance and control rotations around the coronal plane. This might be even more pronounced in unilateral amputee sprinting due to the weight and stiffness asymmetry between the two legs. Hence, we expect that an extension of the models to three dimensions will reveal substantial differences in the contribution of the arms and the angular momentum control.

## Acknowledgments

We want to thank the Simulation and Optimization research group of the Interdisciplinary Center for Scientific Computing at Heidelberg University for giving us the possibility to work with MUSCOD-II.

## Supplementary Material

To view supplementary material for this article, please visit <https://doi.org/10.1017/S0263574719000936>.

## References

1. G.-P. Brüggemann, A. Arampatzis, F. Emrich and W. Potthast, "Biomechanics of double transtibial amputee sprinting using dedicated sprinting prostheses," *Sports Technol.* **1**(4–5), 220–227 (2008).
2. P. G. Weyand, M. W. Bundle, C. P. McGowan, A. Grabowski, M. B. Brown, R. Kram and H. Herr, "The fastest runner on artificial legs: different limbs, similar function?" *J. Appl. Physiol.* **107**(3), 903–911 (2009).
3. B. Burkett, M. McNamee and W. Potthast, "Shifting boundaries in sports technology and disability: equal rights or unfair advantage in the case of oscar pistorius?" *Disabil. Soc.* **26**(5), 643–654 (2011).
4. C. P. McGowan, A. Grabowski, M. B. Brown, R. Kram and H. Herr, "Counterpoint: Artificial legs do not make artificially fast running speeds possible," *J. Appl. Physiol.* **108**(4), 1012–1014 (2010).
5. V. Wank and V. Keppler, "Vor- und Nachteile von Sportlern mit Hochleistungsprothesen im Vergleich zu nichtbehinderten Athleten," *Deutsche Zeitschrift für Sportmedizin* **66**(11), 287–293 (2015).
6. P. G. Weyand and M. W. Bundle, "Point: Artificial legs do make artificially fast running speeds possible," *J. Appl. Physiol.* **108**(4), 1011–1012 (2010).
7. K. Mombaur, "A mathematical study of sprinting on artificial legs," **In: Modeling, Simulation and Optimization of Complex Processes - HPSC 2012** (Springer International Publishing, Cham, 2014) pp. 157–168.
8. G. Strutzenberger, A. Brazil, H. von Lieres und Wilkau, D. Davies, J. Funken, R. Müller, T. Excell, C. Willson, S. Willwacher, W. Potthast, H. Schwameder and G. Irwin, "1st and 2nd step characteristics preceding the sprint start in amputee sprinting," *34th International Conference on Biomechanics in Sports*, Tsukuba, Japan (2016) pp. 964–967.
9. P. Taboga, A. M. Grabowski, P. E. di Prampero and R. Kram, "Optimal starting block configuration in sprint running: A comparison of biological and prosthetic legs," *J. Appl. Biomech.* **30**(3), 381–389 (2014).
10. S. Willwacher, V. Herrmann, K. Heinrich, J. Funken, G. Strutzenberger, J.-P. Goldmann, B. Braunstein, A. Brazil, G. Irwin, W. Potthast and G.-P. Brüggemann, "Sprint start kinetics of amputee and non-amputee sprinters," *PLoS ONE* **11**(11), e0166219 (2016).
11. J. Funken, K. Heinrich, S. Willwacher, R. Müller and W. Potthast, "Amputation side and site determine the performance capacity in paralympic curve sprinting," *34th International Conference on Biomechanics in Sports*, Tsukuba, Japan (2016) pp. 589–592.
12. H. Hobara, Y. Kobayashi and M. Mochimaru, "Spatiotemporal Variables of Able-Bodied and Amputee Sprint in Men's 100-m Sprint," *Int. J. Sports Med.* **36**, 494–497 (2015).
13. R. V. Mann, "A kinetic analysis of sprinting," *Med. Sci. Sports Exercise* **13**(5), 325–328 (1981).
14. H. Hobara, B. S. Baum, H.-J. Kwon, R. H. Miller, T. Ogata, Y. H. Kim and J. K. Shim, "Amputee locomotion: Spring-like leg behavior and stiffness regulation using running-specific prostheses," *J. Biomech.* **46**, 2483–2489 (2013).
15. F. Kugler and L. Janshen, "Body position determines propulsive forces in accelerated running," *J. Biomech.* **43**, 343–348 (2010).
16. S. Willwacher, J. Funken, K. Heinrich, T. Alt, R. Müller and W. Potthast, "Free moment application by athletes with and without amputations in linear and curved sprinting," *35th International Conference on Biomechanics in Sports, Cologne, Germany*, vol. 35 (2017) pp. 847–850.
17. P. G. Weyand, D. B. Sternlight, M. J. Bellizzi and S. Wright, "Faster top running speeds are achieved with greater ground forces not more rapid leg movements," *J. Appl. Physiol.* **89**, 1991–1999 (2000).
18. A. L. Kleesattel, D. Clever, J. Funken, W. Potthast and K. Mombaur, "Modeling and Optimal Control of Able-Bodied and Unilateral Amputee Running," *35th International Conference on Biomechanics in Sports, Cologne, Germany*, vol. 35 (2017) pp. 164–167.
19. B. K. Higginson, "Methods of running gait analysis," *Curr. Sports Med. Rep.* **8**(3), 136–141 (2009).
20. M. Günther, V. A. Sholukha, D. Kessler, V. Wank and R. Blickhan, "Dealing with skin motion and wobbling mass in inverse dynamics," *J. Mech. Med. Biol.* **3**(3–4), 309–335 (2003).
21. S. L. Delp, F. C. Anderson, A. S. Arnold, P. Loan, A. Habib, C. T. John, E. Guendelman and D. G. Thelen, "Opensim: Open-source software to create and analyze dynamic simulations of movement," *IEEE Trans. Biomed. Eng.* **54**(11), 1940–1950 (2007).
22. M. L. Felis, K. Mombaur and A. Berthoz, "An optimal control approach to reconstruct human gait dynamics from kinematic data," *IEEE RAS International Conference on Humanoids Robots*, Seoul, Korea (2015) pp. 1044–1051.
23. Y.-C. Lin and M. G. Pandy, "Three-dimensional data-tracking dynamic optimization simulations of human locomotion generated by direct collocation," *J. Biomech.* **59**, 1–8 (2017).
24. R. H. Miller, B. R. Umberger, J. Hamill and G. E. Caldwell, "Evaluation of the minimum energy hypothesis and other potential optimality criteria for human running," *Proc. R. Soc. London B: Biol. Sci.* **279**(1733), 1498–1505 (2011).
25. S. Willwacher, J. Funken, K. Heinrich, R. Müller, H. Hobara, A. M. Grabowski, G.-P. Brüggemann and W. Potthast, "Elite long jumpers with below the knee prostheses approach the board slower, but take-off more effectively than non-amputee athletes," *Sci. Rep.* **7**(1), 16058 (2017).
26. P. de Leva, "Adjustments to Zatsiorsky-Seluyanov's segment inertia parameters," *J. Biomech.* **29**(9), 1223–1230 (1996).
27. G. Schultz and K. Mombaur, "Modeling and optimal control of human-like running," *Trans. Mechatron.* **15**(5), 783–792 (2010).
28. M. L. Felis, "RBDL: An efficient rigid-body dynamics library using recursive algorithms," *Auton. Robots* **41**(2), 495–511 (2017).

29. H. G. Bock and K.-J. Plittm, "A Multiple Shooting Algorithm for Direct Solution of Optimal Control Problems," *Proceedings of the 9th IFAC World Congress*, Budapest, Hungary (1984) pp. 242–247.
30. D. B. Leineweber, I. Bauer, H. G. Bock and J. P. Schlöder, "An efficient multiple shooting based reduced SQP strategy for large-scale dynamic process optimization (Parts I and II)," *Comput. Chem. Eng.* **27**(2), 157–174 (2003).
31. K. P. Clark, L. J. Ryan and P. G. Weyand, "A general relationship links gait mechanics and running ground reaction forces," *J. Exp. Biol.* **220**, 247–258 (2017).
32. H. Geyer, A. Seyfarth and R. Blickhan, "Compliant leg behaviour explains basic dynamics of walking and running," *Proc. R. Soc. London B: Biol. Sci.* **273**(1603), 2861–2867 (2006).
33. I. N. Bezodis, D. G. Kerwin and A. I. T. Salo, "Lower-limb mechanics during the support phase of maximum-velocity sprint running," *Med. Sci. Sports Exercise* **40**(4), 707–715 (2008).
34. S. Stafilidis and A. Arampatzis, "Track compliance does not affect sprinting performance," *J. Sports Sci.* **25**(13), 1479–1490 (2007).
35. A. G. Schache, P. D. Blanch, T. W. Dorn, N. A. T. Brown, D. Rosemond and M. G. Pandy, "Effect of running speed on lower limb joint kinetics," *Med. Sci. Sports Exercise* **43**(7), 1260–1271 (2011).
36. C. P. McGowan, A. M. Grabowski, W. J. McDermott, H. M. Herr and R. Kram, "Leg stiffness of sprinters using running-specific prostheses," *J. R. Soc. Interf.* **9**(73), 1975–1982 (2012).
37. A. L. Kleesattel, W. Potthast and K. Mombaur, "Towards a Better Understanding of Human Sprinting Motions With and Without Prostheses," *IEEE RAS International Conference on Humanoid Robots*, Birmingham, UK (2017) pp. 158–164.
38. A. L. Emonds and K. Mombaur, "Inverse Optimal Control Based Enhancement of Sprinting Motion Analysis With and Without Running-Specific Prostheses," *IEEE RAS/EMBS International Conference on Biomedical Robotics and Biomechanics* (2018) pp. 556–562, Enschede, Netherlands: IEEE RAS/EMBS.